

Article

A GIS Plugin for the Assessment of Deformations in Existing Bridge Portfolios via MTInSAR Data

Mirko Calò , Sergio Ruggieri *, Andrea Nettis  and Giuseppina Uva 

Department DICASTeCh, Polytechnic University of Bari, Via Orabona, 4, 70126 Bari, Italy; mirko.calo@poliba.it (M.C.); andrea.nettis@poliba.it (A.N.); giuseppina.uva@poliba.it (G.U.)

* Correspondence: sergio.ruggieri@poliba.it

Abstract: The paper presents a GIS plugin, named Bridge Assessment System via MTInSAR (BAS-MTInSAR), aimed at assessing deformations in existing simply supported concrete girder bridges through Multi-Temporal Interferometry Synthetic Aperture Radar (MTInSAR). Existing bridges require continuous maintenance to ensure functionality toward external effects undermining the safety of these structures, such as aging, material degradation, and environmental factors. Although effective and standardized methodologies exist (e.g., structural monitoring, periodic onsite inspections), new emerging technologies could be employed to provide time- and cost-effective information on the current state of structures and to drive prompt interventions to mitigate risk. One example is represented by MTInSAR data, which can provide near-continuous information about structural displacements over time. To easily manage these data, the paper presents BAS-MTInSAR. The tool allows users to insert information of the focused bridge (displacement time series, structural information, temperature data) and, through a user-friendly GUI, observe the occurrence of abnormal deformations. In addition, the tool implements a procedure of multisource data management and defines proper thresholds to assess bridge behavior against current code prescriptions. BAS-MTInSAR is fully described throughout the text and was tested on a real case study, showing the main potentialities of the tool in managing bridge portfolios.

Keywords: existing bridges; bridge assessment; geographic information system; multi-temporal interferometry synthetic aperture radar



Citation: Calò, M.; Ruggieri, S.; Nettis, A.; Uva, G. A GIS Plugin for the Assessment of Deformations in Existing Bridge Portfolios via MTInSAR Data. *Remote Sens.* **2024**, *16*, 4293. <https://doi.org/10.3390/rs16224293>

Academic Editors: Joan Ramon Casas Rius, Necati Catbas, Rolando A. Chacón and Daniele Zonta

Received: 18 September 2024
Revised: 15 November 2024
Accepted: 15 November 2024
Published: 18 November 2024



Copyright: © 2024 by the authors. Licensee MDPI, Basel, Switzerland. This article is an open access article distributed under the terms and conditions of the Creative Commons Attribution (CC BY) license (<https://creativecommons.org/licenses/by/4.0/>).

1. Introduction

Bridges are core assets in transportation networks and serve for overpassing natural disconnections (e.g., rivers, valleys) or man-made obstacles (e.g., railways, motorways). Continuous maintenance of existing bridges is fundamental to preserving their functionality toward external actions and to ensure the safety of users. In fact, a negligent approach could lead to intangible economic losses and casualties, as shown by the recent black chronicles, which reported the collapse of important bridges such as the Polcevera viaduct [1] (2018, Genoa, Italy) and the Albiano-Magra viaduct [2] (2020, Albiano-Magra, Italy). Different causes can lead to disruptive phenomena until collapse, such as unexpected natural hazards (e.g., seismic, geological), leading to reduce the health state of structures, like aging, material degradation, and adverse environmental conditions.

The management of bridge portfolios is nowadays a primary issue, and it is addressed by national governments, which should drive management companies through new and reliable technical codes and guidelines [3,4]. Although these strategies are effective, they require high efforts and costs and for sure cannot be applied by transportation management companies to large bridge portfolios (e.g., the national highway autonomous company, ANAS, manages more than 10,000 bridges in Italy). Moreover, the required actions to preserve existing bridge portfolios should be taken in a timely manner and frequently,

but the suggested activities are usually slowly performed, especially if considering the often-limited expected residual life of the considered bridges.

To support and improve assessment procedures of existing bridge portfolios, new technologies can be explored, such as cost-effective ones that allow near-continuous monitoring of structural health. One possible option is represented by Multi-Temporal Interferometry Synthetic Aperture Radar (MTInSAR), a remote sensing technique exploiting image stacks acquired by Synthetic Aperture Radar (SAR) sensors. MTInSAR data are used to detect displacements related to scatterers on the Earth's surface, mostly associated with parts of man-made structures (e.g., buildings and bridges) [5]. The displacements are recorded along the line-of-sight (LoS) and are used to study slow kinematic motions. The fields of application of this technique are wide and range from evaluating effects of landslide and subsidence on structures [6–8] to monitoring structural displacements for a single [2,9–11] or group [12–15] of structures.

Looking at the available scientific literature, this technique shows good potentiality for the purpose of bridge displacements assessment, but several hurdles can be faced in the management and interpretation of data. In fact, a correct evaluation of the output depends on the data collection and aggregation (considering different data sources), which require articulated computational steps, often difficult to replicate for each bridge within a considered portfolio manually. Moreover, the application of SAR data for structural assessment is limited by the interdisciplinary nature of the technical knowledge required, reducing the number of potential users, especially in the field of professional practice. A viable option to manage georeferenced data as MTInSAR products (e.g., mapping, theming, visualization, storing) is represented by geographic information systems (GIS). As discussed in Section 2, a GIS is used to understand patterns, relationships, and to perform calculations through a mathematical and geometrical processing toolbox [15], with the advantage of being opensource [16].

Given the advantages of GIS and the possibility of enclosing in a single environment all of the tools needed for assessing deformations in existing bridges via MTInSAR, this paper proposes a GIS plugin (related to the QGIS software package) named Bridge Assessment System via MTInSAR (BAS-MTInSAR). BAS-MTInSAR was developed for simply supported concrete girder bridges as the most widespread bridge typology in Italy and Europe. Through its graphic user interface (GUI), the tool allows the user to: (i) collect input information, such as bridge geometry, MTInSAR data, and temperature data; (ii) explore scatterer positions, attributes, and LoS-oriented displacement time series for informed selection; (iii) compute displacement profiles of the bridge along its deformation axes, defined according to their service condition; (iv) observe seasonal and trend components of displacement profiles; (v) evaluate deformation scenarios considering code prescriptions and available literature; (vi) gather insights and warnings about possible causes of abnormal deformations; (vii) update deformation scenario evaluation results given the availability of new onsite survey as well as SAR data; (viii) track the evolution of bridges through statistics and saved results. All of these services are available in BAS-MTInSAR and its Python modules. The main advantages brought by BAS-MTInSAR are its opensource nature, which allows its Python modules to be used separately in similar applications, as long as they are related to the use of SAR data for structural assessment, or to scale its contents by adding new features. Moreover, for the development of BAS-MTInSAR, a new evaluation scenario and the structural interpretation of bridge displacements are introduced to improve the state-of-the-art about the use of MTInSAR data for displacement monitoring of bridges [2,12]. This functionality provides useful insights for practitioners and bridge inspectors during onsite survey campaigns about the considered bridge typology.

After this brief introduction, Section 2 reports the state-of-the-art about the use of SAR data through GIS tools, Section 3 present the full description of BAS-MTInSAR functionalities and its GUI, Section 4 reports the application of the tool to a case study, and Section 5 provide conclusions and further developments.

2. Integration of Satellite Data in GIS Environment: State-of-the-Art

GIS is a powerful tool in several research fields and applications for spatial analysis and informed decision making through aggregation, management, and visualization of georeferenced data. When referring to displacement monitoring through MTInSAR data, the scientific literature proposes different examples showing the combination and analysis of multi-source data in the GIS environment.

One of the most popular applications in which MTInSAR data are employed is the ground motion detection of large areas. Bordoni et al. [7] and Meisina et al. [8] focused on this topic by post-processing interferometry SAR (InSAR) data through a working chain based on different opensource software. In their work, the displacement time series accuracy of Persistent Scatterers (PS) was evaluated to improve the reliability of results and the identification of areas characterized by anomalous displacements was achieved by aggregating PS displacement time series with terrain data (i.e., geological, geotechnical, hydrogeological, and land use information) and digital elevation models (DEMs) through GIS tools.

Talking about infrastructure systems, DePrekel et al. [14] and Macchiarulo et al. [15] studied the deformation of a wide area through MTInSAR data. Using GIS tools, zones of maximum ground displacement were identified from SAR data and the use of a descriptive database of road networks was useful for identifying assets toward local analysis were performed to describe their deformation mechanism (e.g., long-term downward displacements, correlated with the regional subsidence). The application on real case studies demonstrated that the procedures were suitable for the screening of large transportation networks and for the identification of infrastructures requiring further investigations. Other examples on MTInSAR and GIS data integration for infrastructure displacement monitoring can be found in [17–24].

Although not exhaustive, this brief literature review highlights the main advantages and shortcomings of the integration of satellite data with GIS software, with the possibility of performing different operations. As the main advantage, GIS software allows users to display PS displacement time series through opensource plugins, avoiding the use of external data visualization tools. Furthermore, GIS tools facilitate the geoprocessing of LoS displacements (e.g., projections along desired directions, calculation of displacement velocities) and the integration of free road maps inventories, such as OpenStreetMap, allows the user to properly select PS in an easier and automatic way. Close to the above advantages, some issues should be highlighted. Most of the above operations require time and manual actions by users, as well as basic knowledge of programming languages. To facilitate the automation and the assessment of bridge displacements at the portfolio scale through MTInSAR data, a new and comprehensive GIS plugin is necessary, able also to automatically check the occurred displacement toward specific thresholds (e.g., related to deformation scenarios, based on code prescriptions, and the available literature) for the purpose of early warning. With this goal in mind, BAS-MTInSAR is proposed with a full description of its GUI, functionalities, and working principles.

3. BAS-MTInSAR: Definition of a New GIS Plugin

BAS-MTInSAR was developed for QGIS application and was idealized at this stage for simply supported concrete girder bridges, as the most widespread bridge typology in Italy and Europe. The framework at the base of BAS-MTInSAR is shown in Figure 1. Section 3.1 reports the analytical description of the steps of the automated analysis and Section 3.2 presents the GUI.

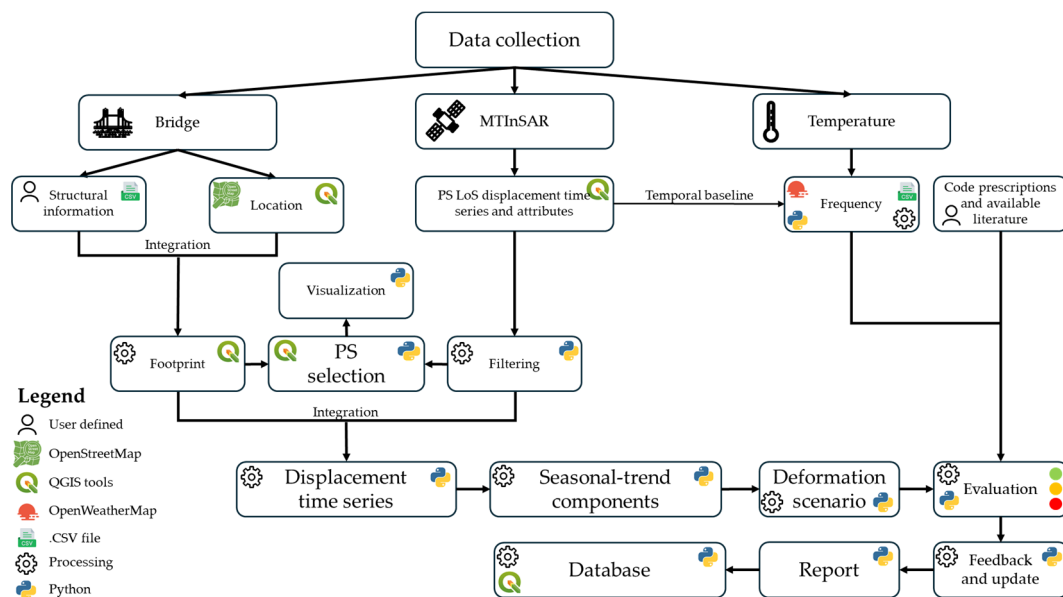


Figure 1. Framework of BAS-MTInSAR.

3.1. Analytical Steps of BAS-MTInSAR

BAS-MTInSAR is designed to automate and guide practitioners toward the application of laborious analytical steps for structural interpretation of bridge displacements, requiring interdisciplinary technical knowledge. The modules implemented in the plugin GUI take advantage of the most promising techniques reported in the scientific literature on the topic [12] and extend their content, providing an additional displacement scenario and structural interpretation of bridge displacement time series. The following steps are required to achieve structural assessment through MTInSAR data.

STEP 1: Data collection and PS selection.

Step 1 regards the collection of input data about the geometrical (e.g., bridge centerline, number of spans, deck and beam sections, bearing distribution), mechanical (e.g., elastic modulus, E_c , and coefficient of thermal expansion, α_{CTE} , of concrete), and location (e.g., latitude, longitude, altitude) characteristics of the bridge. Temperature data (e.g., average temperatures recorded at weather stations near the bridge) and satellite data of the COSMO Sky-Med type (i.e., at the best spatial resolution, $3\text{ m} \times 3\text{ m}$) from ascending (ASC) and descending (DSC) acquisition geometries are needed as well. The latter can be used in the proposed analysis only if processed by means of MTInSAR algorithms. From the processing of the SAR data, PS are obtained with their LoS-oriented displacement time series and attributes (e.g., location and coherence). The location and some geometrical characteristics of the bridge (bridge centerline, deck width, altitude) are used to define the georeferenced footprint of the structure. The other geometrical characteristics, like beam and deck sections and the bearing distribution, are exploited in combination with the mechanical features of the bridge to describe the expected behavior of the deck under service conditions (see Step 4).

Once the bridge is identified, each span is subdivided into three sub-regions (i.e., the two at the side in correspondence of the bearings, 1st and 3rd sub-regions, and one in the middle at midspan, 2nd sub-region, Figure 2) considering their different structural behaviors under service conditions, as shown in Step 4.

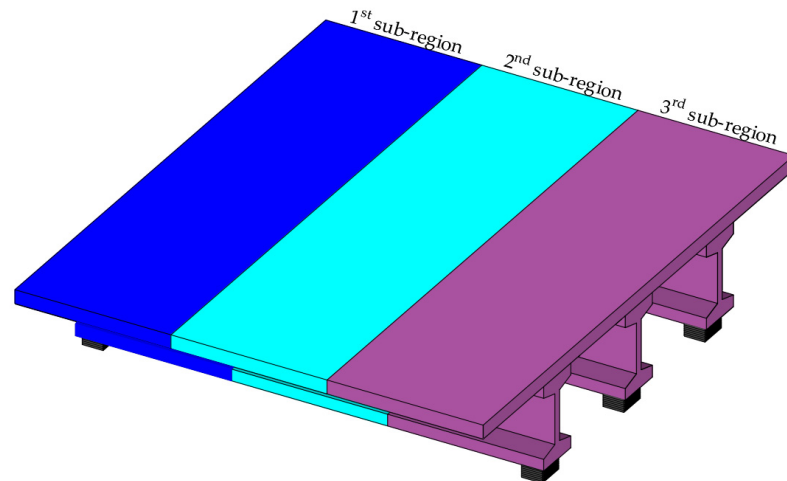


Figure 2. Example of simply supported deck divided in three equally distributed sub-regions: 1st sub-region (blue) near the pinned support, 2nd sub-region (cyan) at midspan, and 3rd sub-region (purple) near the roller support. The bearing typology shown in the example is unbonded elastomeric, where the greater the bearing height, the lower the translation stiffness (i.e., higher displacement).

After elaboration of the satellite data via MTInSAR algorithm, the obtained PS are carefully selected to provide bridge-related information. For this purpose, hierarchical selection criteria are proposed based on: (i) localization of PS and mutual position with the footprint (in plan and height), considering inaccuracies due to SAR acquisition geometry and MTInSAR algorithms elaborations; (ii) coherence of the PS; (iii) velocities along the LoS, V_{LoS} . At the end of this step of the analysis, the centroid of each sub-region is described by two average displacement time series along the LoS, d_{LoS} , derived from the retained PS, one for each acquisition geometry (i.e., ASC and DSC). In addition, time sampling processing of the time series is required to align the data obtained from the ASC and DSC datasets for subsequent combination in Step 2.

STEP 2: Displacement time series along bridge main axes.

Disposing of the two time series for each centroid of the sub-regions, the related d_{LoS} are combined and projected in a new reference system, named L-T-V, characterizing the bridge displacement components under service conditions. The longitudinal, L , transverse, T , and vertical, V , directions describe a right-handed cartesian reference system and their displacement components (d_L , d_V , d_T , respectively) are linked to the generic d_{LoS} by the following equation:

$$d_{LoS} = \hat{u}_{LoS} R_V R_T R_L [d_L; d_T; d_V]^T \quad (1)$$

In Equation (1), d_L , d_V , and d_T are unknown terms and R_L , R_V , and R_T are the rotational matrices to perform the projection. These latter are defined by δ , γ , and β angles between the geographical (i.e., East-North-Zenith, E-N-Z) and the L-T-V reference system, respectively, which are specific for each sub-region (Figure 3). It is worth specifying that, given the availability of only two acquisition geometries, one of the unknown terms shall be neglected to solve the system of equations (i.e., one equation for each acquisition geometry). For this bridge typology, the displacements along the T axis, d_T , can be considered negligible compared to the vertical and longitudinal ones.

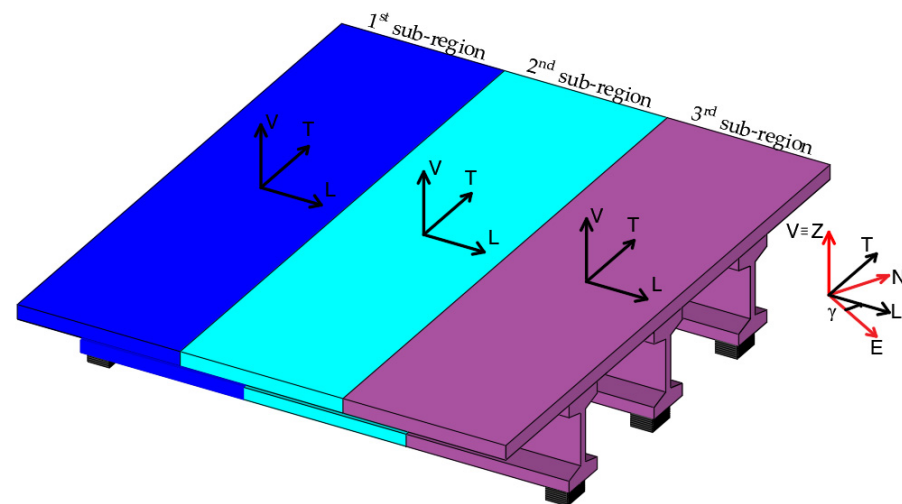


Figure 3. Example of simply supported deck together with L-T-V reference system, in black, for each sub-region. In this case, each sub-region of the bridge is rotated by γ angle with respect to the East direction, reported by the red reference system (i.e., East-North-Zenith).

STEP 3: Definition of seasonality and trend for each displacement component.

At this point, d_L and d_V time series from Step 2 can be processed via mathematical models to derive their trend and seasonality. Step 3 is required because, although useful information can be gained by the time series, the strong trend component (e.g., in the case of subsidence for vertical component) could hide the seasonality. As reported in [12], the use of a literature model called STL (seasonal trend decomposition based on LOESS, [25]) is suggested. An example of such an application is shown in Figure 4a, in which a generic time series of Step 2 is decomposed in three different components: trend, seasonality, and remainder. Still, in the case of bridges characterized by many spans, the computational time required for the decomposition could require faster algorithms, especially in the case of large portfolio screening. Hence, another approach is proposed in which the generic time series is considered as the combination of only trend and seasonality. Specifically, the trend of the displacement time series is computed as a sequence of values obtained by multiplying the slope of the least squares regression method (LSRM), μ in Figure 4b, by the progressive acquisition time. The seasonality is calculated by subtracting the trend component from the original time series. Although less accurate than STL, which uses a moving average algorithm to characterize trend and seasonal components and employs variation over time, this option speeds up the evaluation process. The retrieved components are used in the next step to compare bridge displacements under service conditions and recognize proper displacement scenarios.

STEP 4: Displacement scenarios and structural interpretation.

The information regarding trend and seasonality from Step 3 can be compared with proper thresholds based on the expected behavior of the bridge under service conditions. Generally, this bridge typology can exhibit longitudinal and vertical seasonal displacements. Seasonal longitudinal displacements are related to a constant temperature gradient, ΔT_C , defined on the daily average temperature during the SAR observation time. The threshold, calculated on the base of the analytical model in Figure 5a, considers two extreme configurations of the span: (i) maximum elongation from pinned to roller support under a positive ΔT_C ; (ii) maximum shortening from roller to pinned support under a negative ΔT_C .

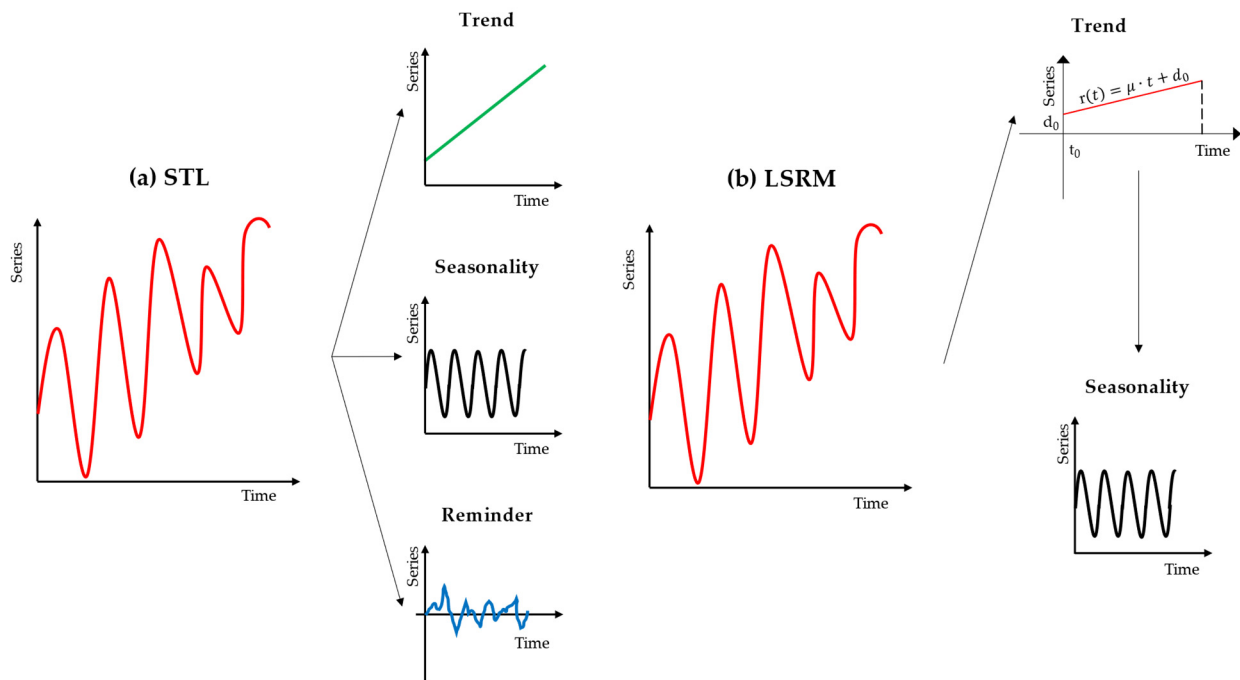


Figure 4. Example of (a) STL and (b) LSRM decompositions of a generic time series from Step 2.

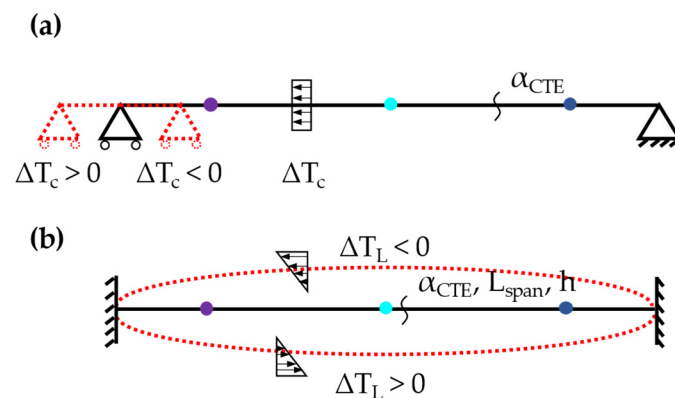


Figure 5. Example of displacement scenario and simple analytical model employed (colored dots represent sub-region centroids): (a) Free longitudinal displacements under constant temperature delta, ΔT_C . The dashed shapes show the deformed configuration of the deck under positive and negative ΔT_C ; (b) Vertical displacements under linear temperature delta, ΔT_L . The dashed shape shows the deformed configuration of the deck under positive and negative ΔT_L .

Vertical seasonal displacements are one of the novelties proposed with BAS-MTInSAR and are linked to a linear temperature gradient, ΔT_L , across the deck section. The use of ΔT_C does not account for the temperature difference between the upper and lower sides of the deck. Indeed, these two regions can be characterized by different temperatures due to solar radiation (the road pavement is hotter than the lower side of the deck) and the presence of snow/thin layer of ice (the road pavement is colder than the lower side of the deck) in summer and winter, respectively. Thus, the additional displacements under ΔT_L are considered only in the vertical direction under a different static scheme reported in Figure 5b. In this case, the deformed shape of the bridge is not characterized by progressive elongation/shortening from pinned to roller support as under ΔT_C . The linear temperature gradient ΔT_L induces an upward deflection during summer and a downward deflection

during winter. The threshold for the vertical seasonal displacement scenario is computed as follows:

$$\delta_v = \frac{\alpha \Delta T_L}{2h} L_{span}^2 \quad (2)$$

where h and L_{span} are the height and length of the deck defined in Step 1, respectively.

Still, other displacement components could characterize the bridge, both longitudinal and vertical, which cannot be considered as service conditions. Regarding the vertical trend components, the difference in cumulative displacements of sub-regions is used to discern among three different deformation scenarios: (i) increasing gravity loads/material degradation; (ii) subsidence; (iii) differential displacements. Each one is characterized by proper thresholds: (i) vertical deflection at midspan (2nd sub-region) under a concentrated load of 600 kN applied in the midspan of an isostatic beam with pinned and roller support constraints and characterized by E_C and the moment of inertia around the transverse axis, J_T ; (ii) and (iii) the three ranges of velocity. These latter are defined as: (a) low velocity below, 2 mm/y; (b) medium velocity, 2–10 mm/y; (iii) high velocity, above 10 mm/y.

The longitudinal trend component scenario is a novelty proposed with BAS-MTInSAR. In this case, the deformation scenario is related to landslides and the range of velocities for vertical trend scenarios (ii) and (iii) are extended to the longitudinal trend scenario. The threshold is compared to the absolute value of the average velocities of the sub-regions.

To provide a structural interpretation of the displacement time series and insights for practitioners and bridge inspectors, the characteristics of bridges collected during Step 1 are considered. In detail, possible bearing malfunctions or wrong information from design documents are recognized starting from the longitudinal seasonal component of the 1st and 3rd sub-regions and the bearing distribution provided to the tool (see Section 3.2). Given the bridge typology under investigation, bearings are usually roller on one side of the span and pinned on the other one to ensure the longitudinal thermal dilation of the deck. Hence, longitudinal displacement due to ΔT_C are incremental and phase-aligned from pinned toward roller bearings for each sub-region. In the case of the longitudinal seasonal components of the 1st and 3rd sub-regions in the reverse phase, the bearings can be assumed as both being rollers. BAS-MTInSAR, checking the bearing distribution with the longitudinal seasonal displacement time series, provides two different attention messages: (i) bearing malfunctions in the case of reverse phase; and (ii) bearing malfunctions/incorrect design documentation in the case of displacements that are incremental from roller toward pinned supports. In both cases, a visual survey is suggested. Other attention messages suggesting visual surveys are prompted for longitudinal and vertical trend components. For the longitudinal one, considering the use of thermal joints, e.g., between spans and abutments on the side of roller bearings, the occurrence of increasing longitudinal displacements higher than 2 mm/y could cause damage. For the vertical component, the potential structural damage identified is different depending on the abovementioned differences between the cumulative displacements of sub-regions and thus displacement scenarios are identified: (i) cracks and/or corrosion are expected on girder beams; (ii) possible damage on transition zones when the bridge deck and the abutments are moving away from each other in the vertical direction; (iii) possible pavement discontinuities due to the vertical relative movement between two adjacent spans or between the side span and abutment.

It is worth noting that the output of the proposed procedure cannot be confused with a structural analysis of bridges in the investigated portfolio, but it aims to provide insights toward the ideal behavior that this bridge typology should exhibit during their service life. Furthermore, the obtained results could be integrated with other tools (e.g., [26]) for the purpose of bridge portfolio assessment.

3.2. BAS-MTInSAR GUI Description

As evidenced in the analytical description of Section 3.1, BAS-MTInSAR is designed to integrate multi-source data. This is possible thanks to Python [27] modules running on version 3.9 (e.g., Pandas, NumPy, Matplotlib, Shapely, Scikit-learn) and QGIS tools

recalled through Python API (i.e., PyQGIS [28]) implementing all of the steps described in the previous Section 3.1. Another strength point of BAS-MTInSAR is its subdivision into separated modules. Each module can be used on its own and extended/integrated with other modules to customize the assessment based on the specific needs. The use of BAS-MTInSAR is proposed with a GUI designed with QT Designer 5.15.2 [29] and including QGIS widgets coded through Qt Designer Python API (i.e., PyQt5 [30]). The main functionalities and the most recurrent elements characterizing the GUI are the following:

- QDialog, top-level window used to store other elements of the GUI.
- QTabWidget, stack of tabbed widgets.
- QFrame, frame to store and organize elements of the GUI.
- QGroupBox, group box frame with a title.
- QComboBox, combines a button with a dropdown list (mainly layer of the QGIS project in this application).
- QgsFileWidget, provides a dialog that allows users to select files or directories (mainly .CSV files in this application).
- QTableWidgetItem, table to store and visualize numerical and categorical data.
- QSpinBox, spin box widget.
- QCheckBox, checkbox with a text label.
- QPushButton, command button to perform actions when pressed.
- QLineEdit, one-line text editor for textual input.
- QTextEdit, used to edit and display both plain and rich text.
- QLabel, text or image display.
- QStackedWidget, a stack of widgets where only one widget is visible at a time.
- QWidget, base class of all user interface objects.
- QListWidget, list of elements.

The main objects of the GUI, i.e., the most used and recurrent in the tool, are illustrated in Figure 6, which reports the indication about the look of the tool, without data. The BAS-MTInSAR plugin is structured in different QDialog windows to optimize its layout and the distribution of functionalities and information. The main QDialog window is named “Bridge Analysis”, Figure 6, containing a QTabWidget of 6 tabs.

The first tab is named “Data collection” (Figure 6) and is used by practitioners to define all of the input information required for the step analysis described in Section 3.1. Starting from the bridge data, organized in three separated QFrame, the minimum requirements to characterize the structure are: (a) geo-localization; (b) beam and deck transverse cross-sections; (c) position and distribution of pinned and roller bearing devices; and (d) E_c . All of the mentioned data are usually available to transportation management companies and stored in various forms depending on their bridge management system. BAS-MTInSAR exploits two ways to import data: (i) shapefiles through QComboBox; and (ii) .CSV files through QgsFileWidget. Depending on the completeness of the imported data, QTableWidgetItem automatically shows a summary of the data, allowing the manual input of missing data. Other automatic operations performed by BAS-MTInSAR, in this first phase, consist of generating the footprint of the bridge and the subdivision of each span into three sub-regions (Figure 2). This process, based on QGIS tools, leads to generate a new polygon shapefile to store the sub-regions characterized with proper attributes (i.e., the ones in the QTableWidgetItem, Figure 7). Indeed, each sub-region is characterized, for example, by height, bearing distribution, beam sections, and by J_T . The latter, calculated from the geometry of beams (“Beam section design” QFrame, only T or double T type) and deck (“Deck section design” QFrame), is required in Step 4 of Section 3.1 for the threshold definition. Figure 7 shows the geometrical quantities used for the definition of J_T . At this stage, such beam typologies are only available for design, which anyway cover a wide range of cases. Further developments of the tool will be aimed at implementing other beam cross-section type definitions (e.g., U-shaped, box).

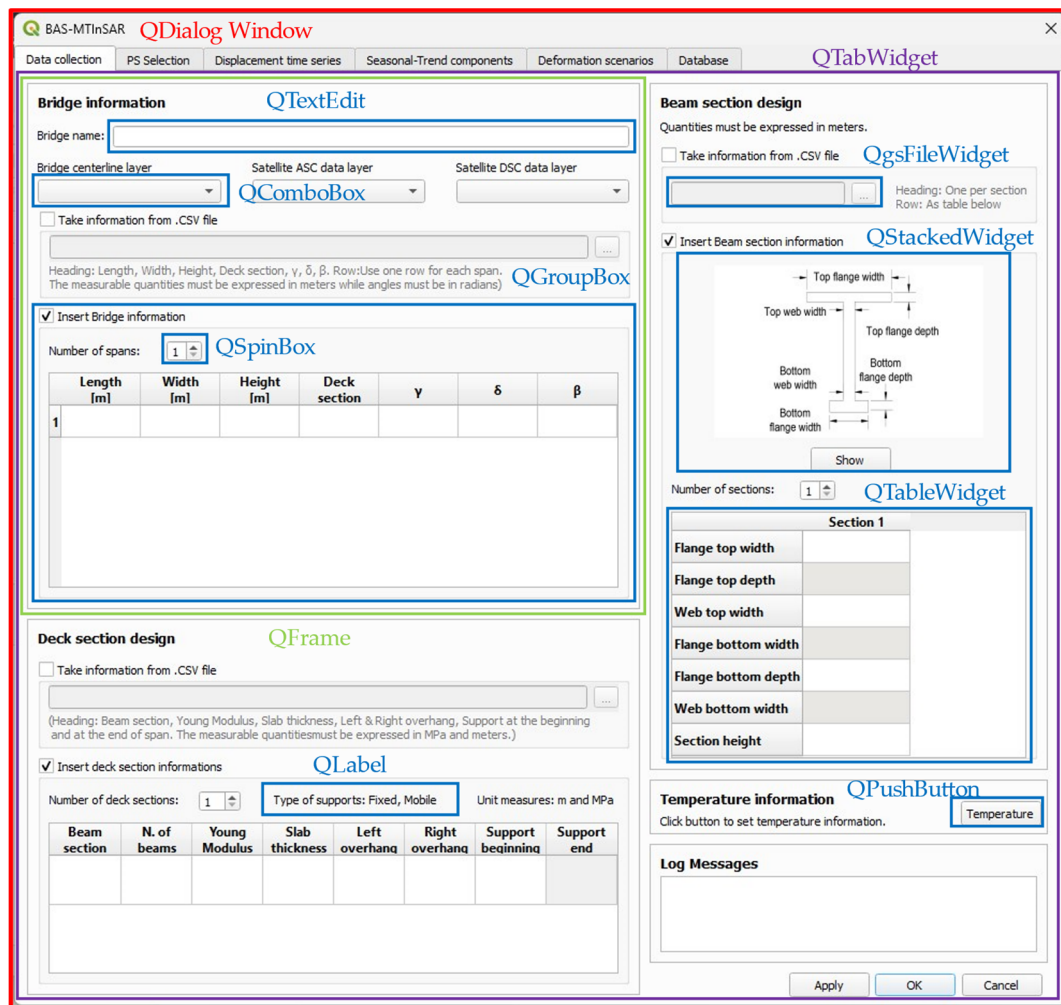


Figure 6. QDialog window named "Bridge Analysis" with boxes showing the most recurrent GUI elements employed in BAS-MTInSAR.

Regarding the other two sources of data, MTInSAR and temperature, similar options are given for their import (i.e., shapefiles for MTInSAR data, one for each acquisition geometry, and .CSV for temperature data). BAS-MTInSAR extracts the information about PS required for Step 1 and 2 of Section 3.1. Lastly, to ease the data collection process, BAS-MTInSAR provides practitioners the possibility to automatically download and process the temperature records from a free API service named OpenWeatherMap [31]. The temperature data definition, included in the "Temperature" QDialog window (see Section 4), can be combined with the use of a cosine temperature model [32] in case of missing daily average temperature values in correspondence of the temporal baseline defined by time sampling processing of the two satellite acquisition geometries. The fitting process, automated in Python, can be shown by the user in the same QDialog window. All of the above steps are tracked in a log messages box, designed with QTextEdit, containing also warnings due to, for example, mismatching of data types (e.g., strings instead of numbers in QTableWidget of bridge information).

The tab named "PS Selection" allows criterion-based PS selection, as described in Step 1 of Section 3.1. The view, organized by spans and acquisition geometries, can be updated every time a new attribute is considered. To enhance the informed selection of PS, the BAS-MTInSAR GUI allows users to observe the PS distribution on the span and, by left clicking on them, to examine their attributes on the right of the plots. Moreover, by right clicking with the cursor on a PS, its LoS displacement time series is prompted in a new QDialog window. Once the practitioner is satisfied with the selection of PS,

the average displacement time series is computed and can be observed in the tab named “Displacement time series”. In this latter tab, organized by spans as in the previous one, BAS-MTInSAR shows the LoS (two Qframe on top) and projected (two Qframe on bottom) average displacement time series of centroids of sub-regions and related quantitative information (i.e., velocities, standard deviation of velocities, and cumulative displacements calculated as velocities in a time interval). It is worth specifying the sign convention of both LoS and projected displacements. LoS displacements are considered positive toward the satellite [33], projected longitudinal components are assumed positive in the direction from the start to the end of the span (this depends on the direction in which the bridge centerline is drawn), and projected vertical components are assumed as positive when upward (Figure 7).

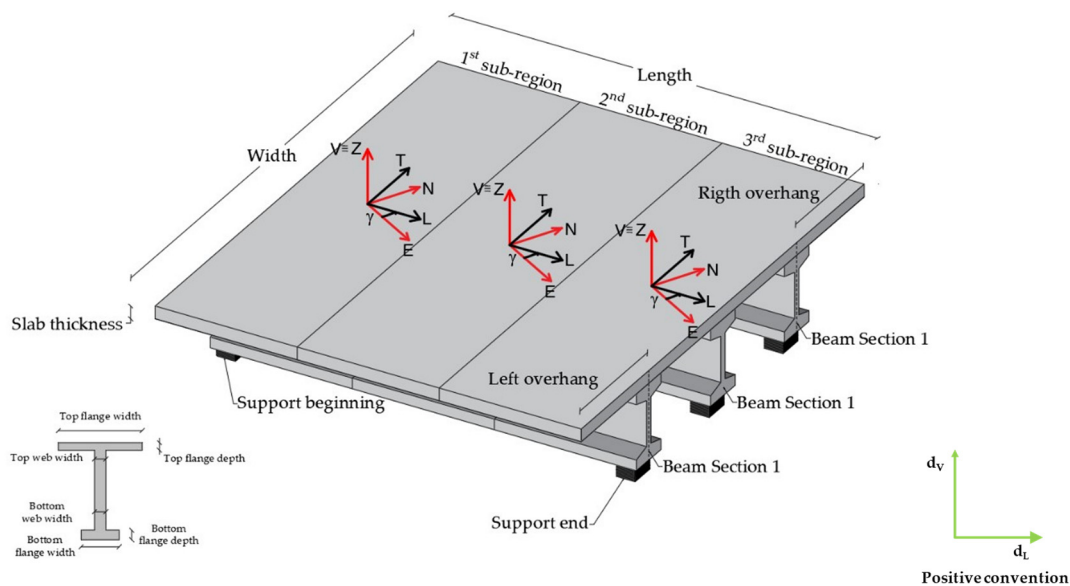


Figure 7. Deck and beam information defined in the QTableWidgets of “Deck section design” and “Beam section design” QFrames for a single span. The green reference system on the right shows the convention sign for bridge displacements of Steps 2 and 3 in the case in which the bridge centerline is drawn from the left to the right, which is from the beginning of the 1st sub-region to the end of the 3rd sub-region in the figure.

To derive additional information about the trend and seasonality of displacements, the tab named “Seasonal-Trend components” is designed. Both STL and LSRM algorithms described in Step 3 of Section 3.1 are available. The results, also in this case organized by spans, are divided in QFrame: (i) the two on the top pertain to the seasonal components, longitudinal and vertical from left to right; and (ii) the two on the bottom pertain to the trend components, in the same order as for the seasonal ones. In this case, QTableWidget records different computed quantities, that is, slope, standard deviation, coefficient of determination of LSRM, and the cumulative displacements.

The evaluation of the deformation scenarios (very important as shown in [34]) and asset management is the core element of BAS-MTInSAR and all data previously elaborated are used in the two tabs named “Deformation scenarios” and “Database”. In “Deformation scenario”, a summary of the required data for the evaluation of scenarios, presented in Step 4 of Section 3.1, and related results are displayed in different QFrames (i.e., one for each displacement component). Also in this case, the representation is provided separately for each span to preserve coherence in the GUI. Near to each threshold value, a graphic symbol (green check, yellow triangle, or red triangle) is shown and, to make checking the results easier and faster, the QLabel thresholds are colored the same as the graphic symbols. The scenario assessment is considered positive (green check) if the thresholds are not overcome in the last two years of observation. Otherwise, an attention (yellow

triangle) or warning (red triangle) message is issued, depending on the number of years in which the thresholds are exceeded for seasonal components, or the magnitude of velocities (classified in three ranges) for the trend components. The attention message includes a description based on the structural assessment explained in Step 4 of Section 3.1. It is worth specifying that possible false alarms could arise due to the inaccuracies of satellite data and their manipulations. For this reason, the deformation scenario results should not be used to detect possible damage but only to support the operation of onsite surveys.

The tab named “Database”, Figure 8, is designed to navigate through the evaluated bridges and to update results. A list of available bridges is designed to select the desired structure and the information automatically saved through shapefiles is recalled and shown (e.g., observation period, status of each deformation scenario, as the worst through the entire bridge, and its summary). Deformation scenario status can be changed through the “Change status” QPushButton, which opens a new QDialog window named “Inspection report”, Figure 9. In this window, users can declare the date of the onsite visual inspection and confirm or clean attention and warning alerts. In the bottom part, a QTableWidgetItem is given for summarizing the number of passed checks and attention and warning marks for each displacement component through the entire database. The “Show on map” QPushButton is used to locate them in the QGIS visualization environment.

Bridges evaluated

New deformation scenario evaluation

Search by name:

List of analysed bridges

- Bridge 1
- Bridge 2
- Bridge 3
- Bridge 4
- Bridge 5
- Fiumicino (Rome)

Selected bridge:

Observation period starts: Edit bridge information

Observation period ends: Edit temperature data

✓ **Longitudinal seasonal component**
 Passed

✓ **Vertical seasonal component**
 Passed

⚠ **Longitudinal trend component**
 ATTENTION: Medium-velocity

⚠ **Trend component**
 WARNING: High-velocity

SPAN 1:

✓ Longitudinal seasonal component overcome in 2018, but within the limits in 2019 and 2020. No reverse phase in seasonality of 1st and 3rd sub-regions as for Roller-Pinned support configuration.

⚠ Longitudinal trend component described as a "Medium-velocity" displacement scenario. ATTENTION: A deformation towards East direction is found, potential damage on longitudinal displacement joints.

✓ Vertical seasonal component overcome in 2018, but within the limits in 2019 and 2020.

✗ Vertical trend component described as a "high-velocity" displacement scenario. Based on the analysis of cumulative displacements and their mutual differences, a subsidence scenario is recognized. WARNING: Survey bridge and surroundings for potential damage on transition zones (abutment).

Summary

	Longitudinal Seasonal Component	Vertical Seasonal Component	Longitudinal Trend Component	Vertical Trend Component
Passed	100	98	81	101
Attention	9	12	30	4
Warning	2	1	0	6

Figure 8. “Database” QTabWidget of “Bridge analysis” QDialog window. Listed bridges (e.g., Bridge 1 in QListWidget) and numbers in the Summary QTableWidgetItem are fictitious and added by the authors for demonstration purposes only. The Fiumicino (Rome) bridge is the one discussed in Section 4.

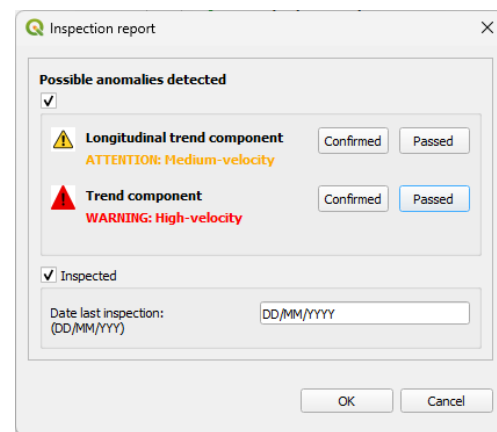


Figure 9. “Inspection report” QDialog window.

4. Application Example on a Real Case Study

This section is aimed at providing an illustrative and technical application of the proposed BAS-MTInSAR plugin on a single-span simply supported concrete girder bridge. About the case study, it is worth noting that the SAR data, elaborated through SPINUA [35], are regarding a bridge for which some details (e.g., name, location) cannot be disclosed by the authors. The bridge should be considered an archetype structure, as its constructive and structural features are representative of existing simply supported concrete bridges built in Europe in the period 1950–1990. However, to show the contents of the GUI, the reserved information was substituted with “****” and, for privacy reasons, a fictitious name is assigned: Fiumicino (Rome).

The single-span bridge in Figure 10 is built in the Fiumicino area, Rome (Italy), well known for its subsidence, as documented by several studies [6,13]. To begin the assessment, a new QGIS project was opened and saved in a directory containing shapefiles of the bridge centerline and of the SPINUA elaborations for ASC and DSC acquisition geometries. Table 1 shows the main features of the COSMO-SkyMed (CKS) datasets. After importing the shapefiles into the project, BAS-MTInSAR was executed. As the first step, the above-mentioned layers were uploaded and incomplete structural information contents were implemented, Figure 11. The double-T beam section was defined and assigned to the deck in a number equal to 10. Environmental temperature data were available from the closest weather station and were processed with the cosine temperature model, Figure 11, due to many missing values along the satellite temporal baseline.

Table 1. Characteristics of the employed SAR datasets.

Satellite	Mode	Spatial Resolution	Pass Type	Time Span	Incidence Angle	Azimuth Angle
CSK	StripMap HIMAGE	3 m × 3 m	ASC	Oct 2017–Nov 2020	33.282	169.373
CSK	StripMap HIMAGE	3 m × 3 m	DSC	Sept 2017–Dec 2020	29.550	11.026

After, PS selection was performed (Figure 12), using only the height criterion due to the few retained PS in each sub-region (i.e., 1st, 2nd, and 3rd) in the case of multi-criteria selection defined in Step 1 of Section 3.1. According to Calò et al. [12], the height criterion only retains PS falling on the footprint and is characterized by the height value comprised between span height plus a tolerance related to the inaccuracies in PS positioning. All of the selected PS were characterized by a negative V_{LoS} value in both acquisition geometries (e.g., L20967P02301 for ASC and L20967P0485 for DSC in Figure 12). Indeed, observing average d_{LoS} in the “Displacement time series” tab (top QFrame in Figure 13), only negative V_{LoS} values were reported, ranging from -12.40 to -13.72 mm/y, together with negative

values of the cumulative displacements, comprised between -37.87 mm and -46.44 mm. Given the convention sign of LoS reported in Section 3.2, PS were moving away from the satellite in both acquisition geometries.

To gather information regarding the displacement components along the bridge axes, the ASC and DSC datasets were combined and projected considering the orientation of the bridge defined by a γ angle equal to 4° , Figure 10. A strong negative vertical component was identified for each sub-region with similar velocities (between -14.29 mm/y and -15.31 mm/y) and cumulative displacements (between -43.65 mm and -46.76 mm) to the ones along the two LoS (bottom right QFrame in Figure 13). This result was expected for two reasons: (a) subsidence phenomena affect the area due to its hydro geomorphological context [6,13]; (b) SAR data reported negative LoS displacements in both acquisition geometries with similar velocities, which was symptomatic of a strong vertical displacement component for the focused structure [33]. Lower values of velocity, 1.7 mm/y, and cumulative displacement, 5.19 mm, were identified for the longitudinal component. Positive values of the longitudinal component were oriented in the West–East direction, considering the drawn direction of the bridge centerline from left to right (West to East), Figure 10.

The seasonality of the vertical projected component was masked by a strong trend, making its evaluation almost impossible. Hence, using the STL algorithm in the “Seasonal-Trend components” tab, Figure 14, the two components were disjointed, confirming the evidence about the vertical trend component. The latter showed maximum velocity and cumulative displacement values, equal to -15.09 mm/y and -46.12 mm, respectively, in correspondence with the 2nd sub-region. On the other hand, a nonlinear longitudinal trend component between 1.06 and 2.34 mm/y was found (from West to East), based on the LSRM over the nonlinear trend. The seasonal components showed almost regular seasonality, as reported in Figure 15 in the proposed tool and shown in Figures 16 and 17 for longitudinal and vertical components, respectively. As reported, this information was used in the “Deformation scenario” evaluation tab, Figure 15, according to the convention sign reported in the green reference system of Figure 18 (positive d_L from left to right, positive d_V upward).

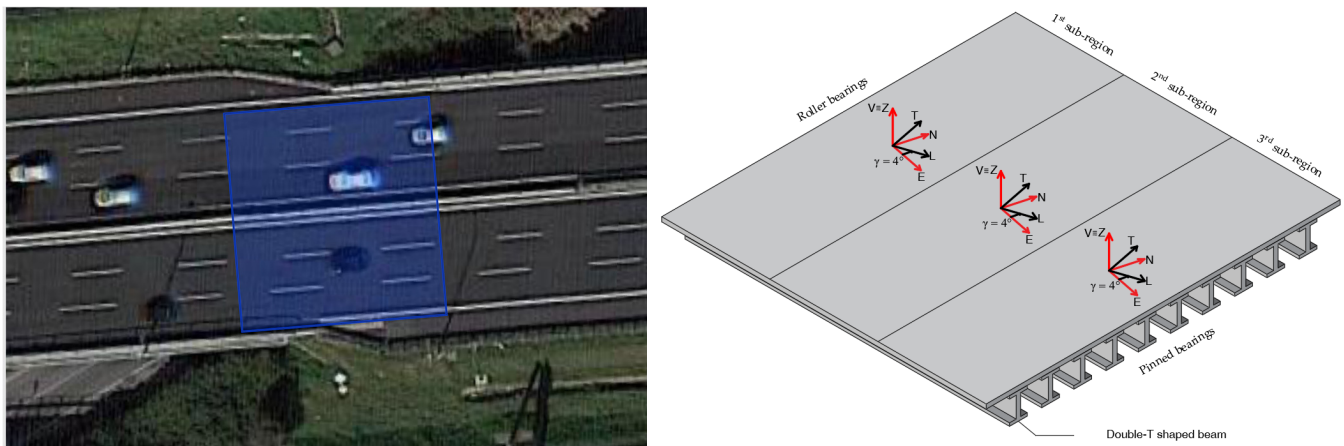


Figure 10. Single-span simply supported concrete girder bridge, Fiumicino, Rome (Italy) and a scale axonometric view. The single-span bridge, characterized by 10 double-T beams of equal sections is divided into three sub-regions (i.e., 1st, 2nd, and 3rd sub-region). The 1st sub-region is characterized by roller bearings, while the 3rd one by pinned bearings. Red and blue lines on the left of the deck represent the expected direction of free longitudinal displacements under constant temperature gradient ΔT_C .

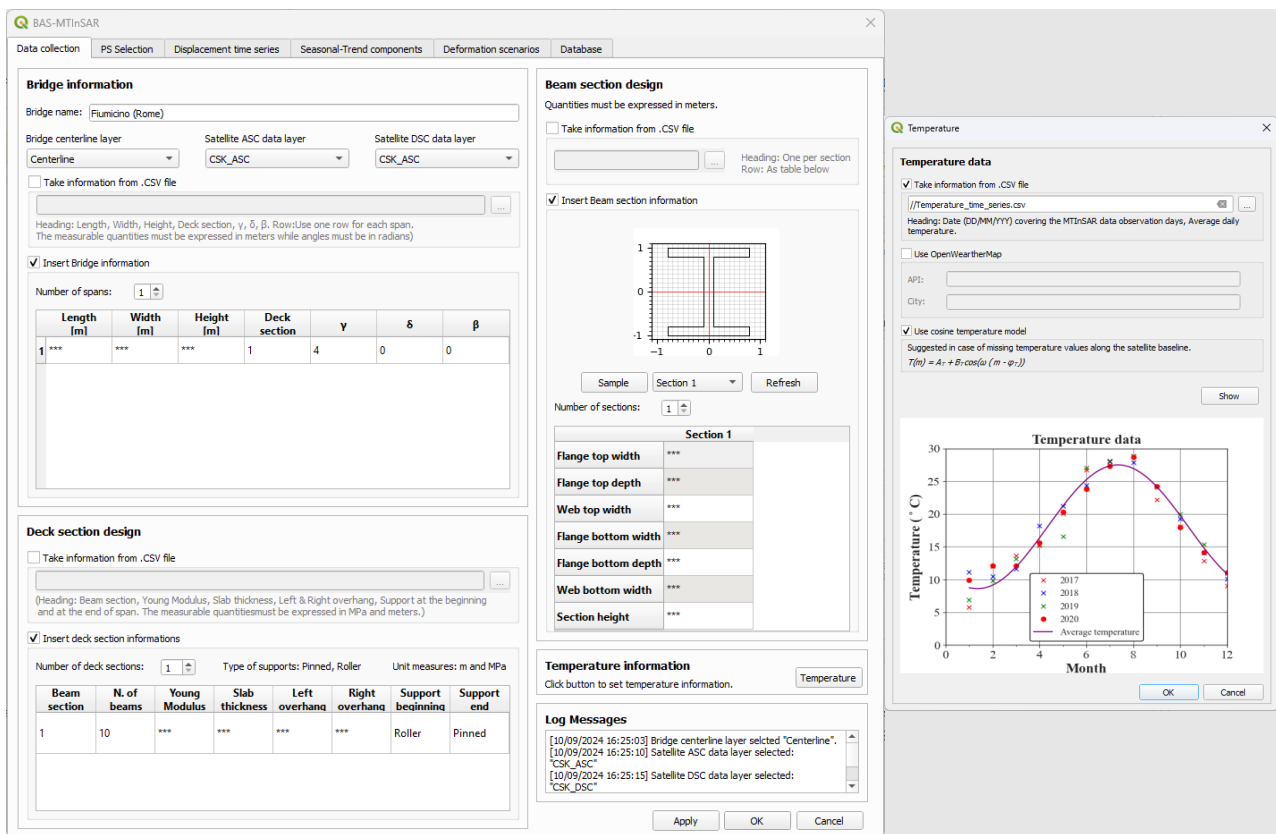


Figure 11. Definition of input data through the “Data collection” QTabWidget of “Bridge analysis” QDialog window and “Temperature” QDialog window. “Deck Section design” and “Beam Section design” are defined according to Figure 3, resulting in Figure 10. Regarding temperature data, the chart shows monthly average temperatures in 2017, 2018, 2019, and 2020 (red cross, blue cross, green cross, and red circle, respectively) used in the cosine temperature model [32]. The purple line is the cosine model, the parameters of which are the average of the model itself fitted over each year of temperature acquisition.

Starting from the seasonal components, the average temperature at the beginning of the observation period (T_{REF}) calculated from the cosine temperature model, Figure 11, was equal to 17.3 °C. From the same data source, exploiting minimum (T_{MIN}) and maximum (T_{MAX}) temperatures in the observation period, 8.6 and 27.5 °C, respectively, two ΔT_C were calculated to define the longitudinal thresholds (herein named positive and negative displacements available). For the vertical seasonal component, a linear gradient temperature of 5 °C was assumed according to code prescriptions [36]. For both seasonal components, the deformation scenario assessment was successful, Figures 16 and 17. In these figures, threshold values (red patches) were reported and their overcoming was registered only in the case of the longitudinal seasonal component, Figure 16, in March and June of 2018. Given the assumption of neglecting the overcoming in the last two years of observation, the assessment was considered positive. The same result can be highlighted for the control performed on bearings. Indeed, based on design documents, the bridge is characterized by roller supports at the beginning of the span (i.e., 1st sub-region) and pinned at its end (i.e., 3rd sub-region). According to this information and to the drawn direction of the bridge centerline, from which the abovementioned convention sign depends, the maximum (i.e., positive) longitudinal seasonal displacements should occur in the coldest months of the year (in Italy, typically from December to February, Figure 11). The ΔT_C of −8.7 °C, equal to $T_{MIN} - T_{REF}$, induced a shortening (negative displacement available) of the deck of 1.9 mm from roller to pinned support, as reported by the blue dashed lines of Figure 18a. On the other hand, during the hottest months of the year (in Italy, typically from June

to August, Figure 11), the ΔT_C of 18.9 °C, equal to $T_{MAX} - T_{REF}$, induced an elongation (positive displacement available) of the deck of 2.3 mm from pinned to roller support, as reported by the red dashed lines of Figure 18a. The phase of the three seasonal longitudinal displacement time series was aligned, and the shortening (positive displacement) was found around January in each year, Figure 16. Thus, the bridge was behaving according to the bearing distribution reported in the design documents, finding a coherence in vertical seasonal displacements. Looking at the static scheme in Figure 5b and time series in Figure 17, a negative ΔT_L of 5 °C inducing positive upward displacement was found in the winter, typical of a deck surface being colder than its lower face. Given the confinement of the vertical seasonal displacements within the proposed thresholds for this assessment scenario, the two thresholds proved to be effective and descriptive of the bridge typology under investigation. Different results were obtained for trend components. A medium-low velocity scenario was found for the longitudinal component toward the East direction, suggesting attention for potential damage of longitudinal displacement joints (i.e., in the case that the bridge deck is moving away from the left abutment in the longitudinal direction). The high-velocity deformation scenario detected on the vertical component was ascribed to subsidence given the negligible difference between the cumulative displacements of sub-regions [12], with a warning to check potential damage on transition zones (i.e., in the case that the bridge deck and the abutments are moving away from each other in the vertical direction). Given the extension of the area affected by hydrogeological phenomena, these occurrences may not be found after the onsite survey and the check might be changed to the “Inspection report” QDialog window, Figure 9. Interested readers can find another application based on BAS-MTInSAR analytical steps in [12].

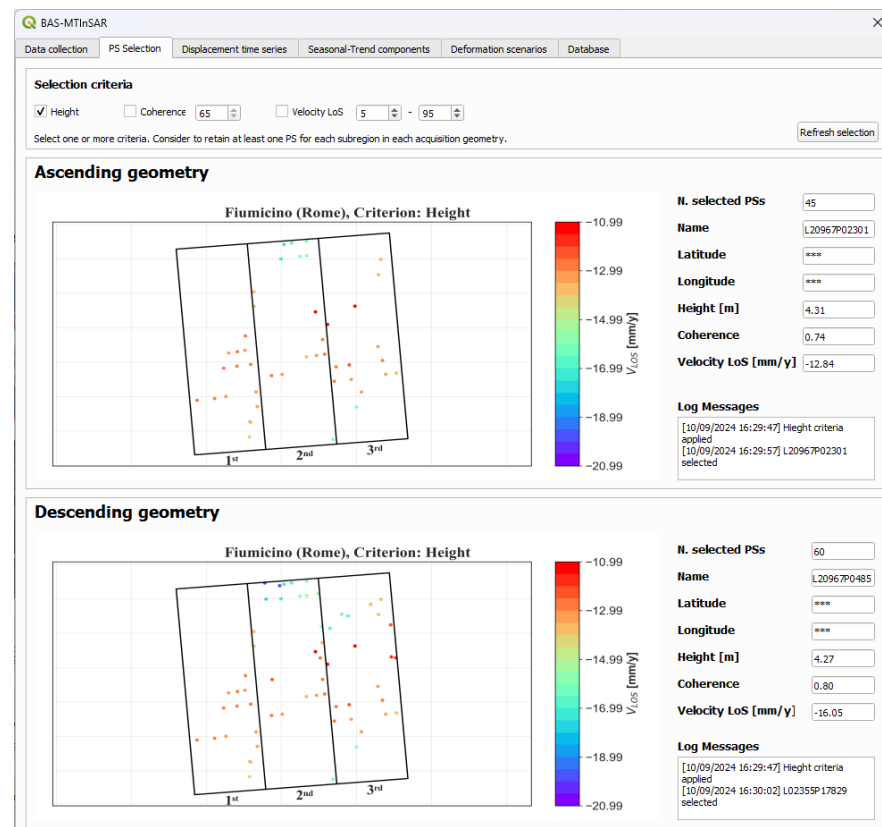


Figure 12. “PS Selection” QTabWidget of “Bridge analysis” QDialog window.

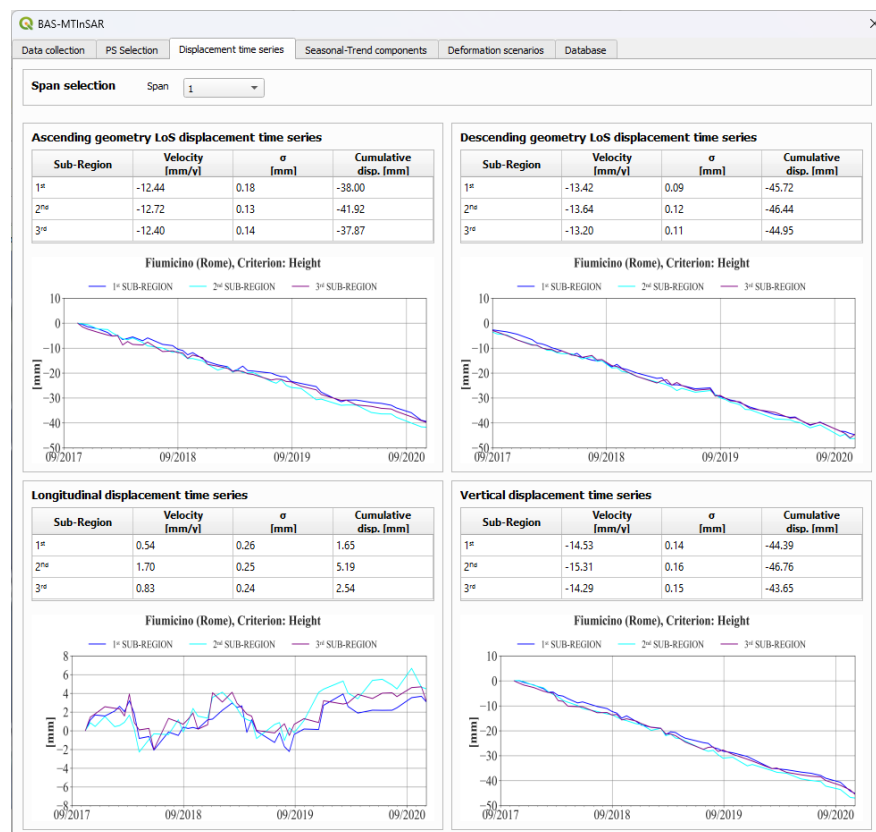


Figure 13. “Displacement time series” QTabWidget of “Bridge analysis” QDialog window.

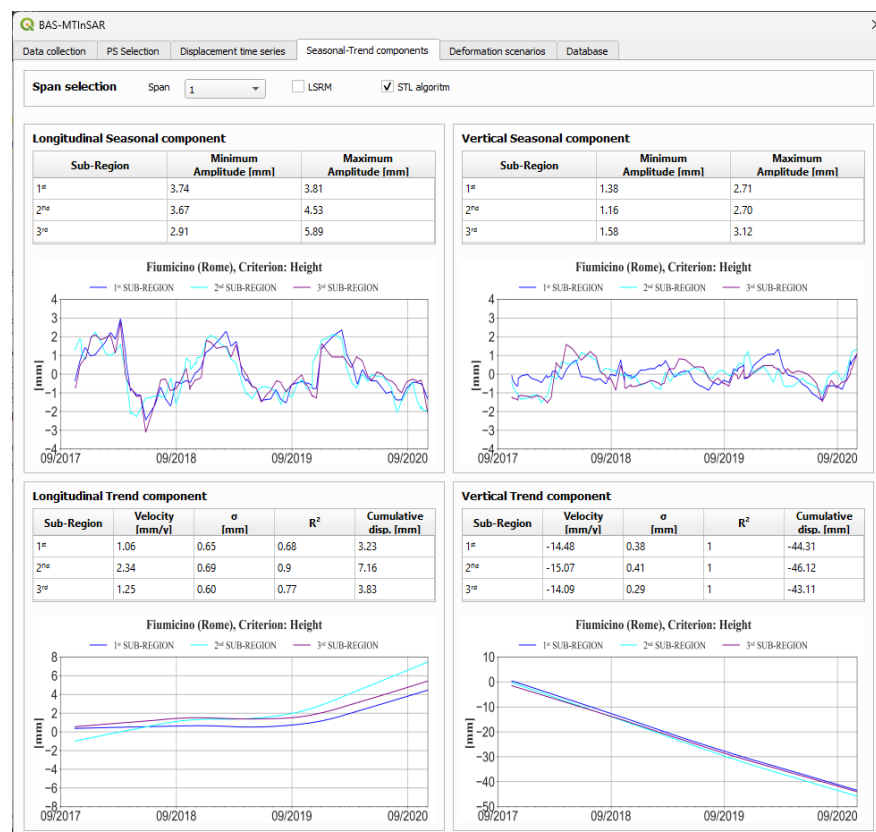


Figure 14. “Seasonal-Trend components” QTabWidget of “Bridge analysis” QDialog window.

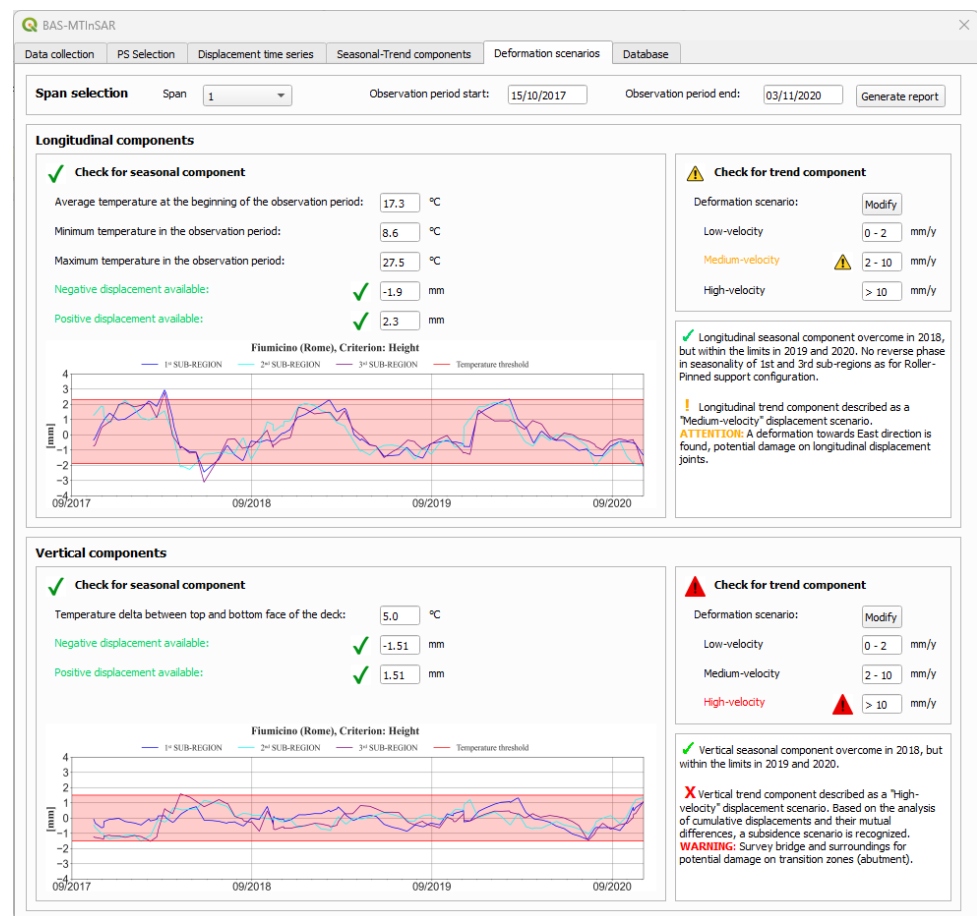


Figure 15. "Deformation scenarios" QTabWidget of "Bridge analysis" QDialog window.

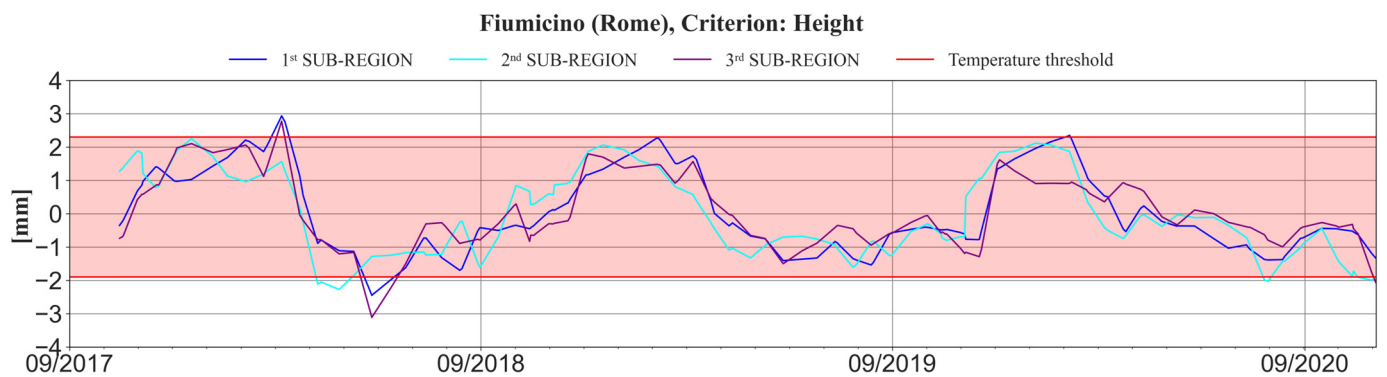


Figure 16. Longitudinal seasonal deformation scenario. Blue, cyan, and purple lines refers to 1st, 2nd, and 3rd sub-regions, while the red patch refers to the range defined by the temperature threshold under ΔT_C .

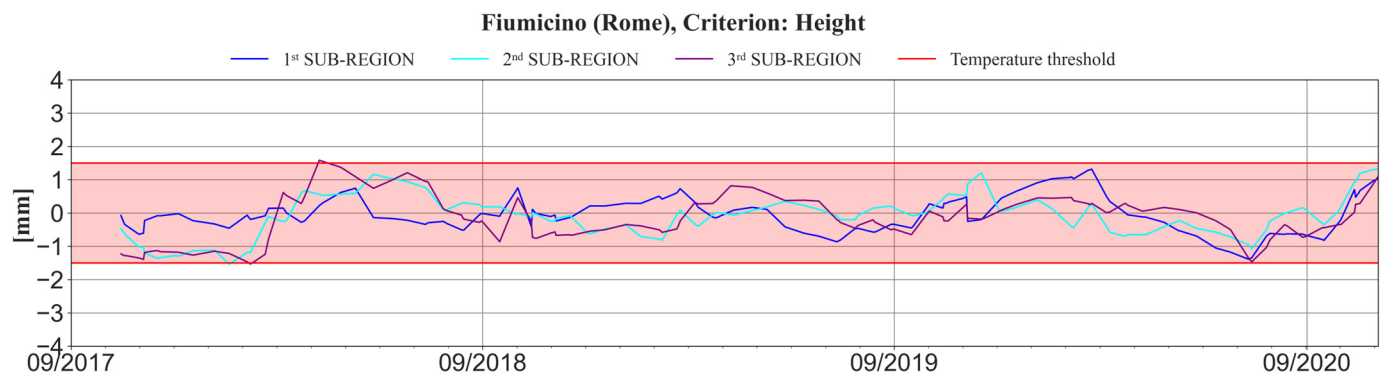


Figure 17. Vertical seasonal deformation scenario. Blue, cyan, and purple lines refers to 1st, 2nd, and 3rd sub-regions, while the red patch refers to the range defined by the temperature threshold under ΔT_L .

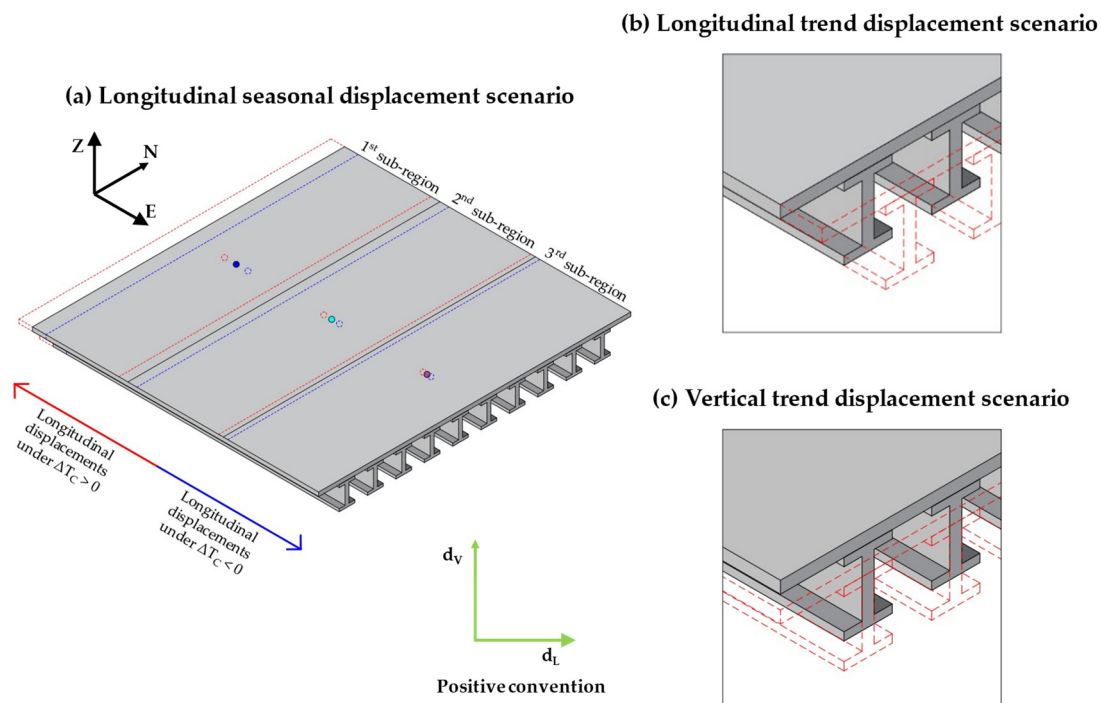


Figure 18. Some of the evaluated bridge displacement scenarios on the Fiumicino (Rome) bridge. (a) Longitudinal seasonal displacement scenario, dashed lines represent the deformed shape of the bridge under ΔT_C . Red lines refer to a positive ΔT_C (negative displacement), blue ones to a negative ΔT_C (positive displacement); (b) Longitudinal trend displacement scenario, focusing on the 3rd sub-region with the dashed lines showing a uniform positive displacement toward the East (black reference system on top left); (c) Vertical trend displacement scenario, focusing on the 3rd sub-region with the dashed lines showing a uniform downward negative displacement. Deformed shapes of the span are not scaled and represented only for description purposes.

5. Conclusions

This paper proposes a GIS plugin named BAS-MTInSAR, designed for the QGIS software package. It is aimed at assessing deformations of existing simply supported concrete girder bridges through Multi-Temporal Interferometry Synthetic Aperture Radar (MTInSAR). The plugin uses Synthetic Aperture Radar data, processed by MTInSAR algorithms, together with structural information and environmental temperatures, to perform near-continuous large-scale monitoring of single structures [6,12,13]. As a main advantage, the Graphic User Interface (GUI) guides users through the assessment chain

involving: (i) definition of all input required; (ii) selection of Persistent Scatterers (PS) based on position and their attributes; (iii) computation of bridge displacement profiles along its deformation axes; (iv) statistical analysis of bridge displacement profiles; (v) full evaluation of deformation scenarios; and (vi) management of bridge portfolio assessment through saved results and statistics. The GUI elements, such as tables and plots, are organized in windows and tabs, allowing the understanding and visualization of the results by users, and limiting the manual operations required and the complexity for practitioners who are not familiar with elaborating MTInSAR data. The integration of structural information, as bearing layout and MTInSAR data, is one of the most interesting innovations proposed by BAS-MTInSAR, which provides feedback on bridge health state (e.g., bearing and longitudinal joints functioning) and indications for timely actions (e.g., onsite surveys). The illustrative application is related to a single-span concrete girder bridge located in Fiumicino (Rome), Italy. The case study section describes the achieved results, recognizing a high-velocity vertical deformation scenario associated with subsidence phenomena documented by the hydro geomorphological context of the area. Still, the thermal dilation of the bridge was recognized and classified within thresholds calculated with simple analytical models based on bridge deck information. Thus, BAS-MTInSAR was demonstrated to be compatible with GIS requirements and for elaborating informed decision making through data aggregation, management, and visualization of georeferenced data.

One of the limitations of BAS-MTInSAR at this stage is related to its development for only simply supported concrete girder bridges characterized by T or double-T beam sections, which covers a wide range of case studies over Italian and European transportation networks. In future developments, the authors will extend the BAS-MTInSAR application field to other bridge typologies and implement other sources of information, such as digital elevation models and landslide/subsidence maps, to address a more accurate assessment depending on the quantity and quality of data at the user's disposal. In the end, it is worth noting that the approaches and data implemented cannot replace traditional monitoring methodologies, considering the limits of characterizing SAR data. Nevertheless, also according to Italian guidelines [4], the approach can be used for large-scale monitoring of bridges within transportation networks, especially for those phenomena that are difficult to survey through visual inspection.

Author Contributions: Conceptualization, M.C., S.R., A.N. and G.U.; methodology, G.U.; software, M.C.; validation, M.C., S.R. and A.N.; formal analysis, S.R.; investigation, S.R.; resources, M.C.; data curation, M.C.; writing—original draft preparation, M.C.; writing—review and editing, S.R. and A.N.; visualization, M.C.; supervision, G.U.; project administration, G.U.; funding acquisition, G.U. All authors have read and agreed to the published version of the manuscript.

Funding: The first author acknowledges funding by the Italian Ministry of University and Research, within the project 'PON-Ricerca e Innovazione-2014–2020, CUP Code (D.M. 10 August 2021, n. 1061): D95F21002340006. The second author acknowledges funding by the Italian Ministry of University and Research, within the project 'PON-Ricerca e Innovazione-2014–2020, CUP Code (D.M. 10 August 2021, n. 1062): D95F21002140006. The third and last author acknowledges the Sustainable Mobility National Research Center (MOST) and received funding from the European Union Next-GenerationEU (PIANO NAZIONALE DI RIPRESA E RESILIENZA (PNRR)—MISSIONE 4 COMPONENTE 2, INVESTIMENTO 1.4—D.D. 1033 17/06/2022, CN00000023)—SPOKE 7 “CCAM, Connected Networks and Smart Infrastructure”—WP4 (CUP D93C22000410001).

Data Availability Statement: The raw data supporting the conclusions of this article will be made available by the authors upon request. The raw data supporting the conclusions of this article will be made available by the authors upon request.

Acknowledgments: The authors acknowledge FABRE consortium for its continuous support. All authors thank Vincenzo Massimi, Vincenzo Barbieri, and Sergio Samarelli from Planetek Italia for providing satellite data.

Conflicts of Interest: The authors declare no conflicts of interest.

References

- Calvi, G.M.; Moratti, M.; O'Reilly, G.J.; Scattarreggia, N.; Monteiro, R.; Malomo, D.; Calvi, P.M.; Pinho, R. Once upon a Time in Italy: The Tale of the Morandi Bridge. *Struct. Eng. Int.* **2018**, *29*, 198–217. [\[CrossRef\]](#)
- Farneti, E.; Cavalagli, N.; Costantini, M.; Trillo, F.; Minati, F.; Venanzi, I.; Ubertini, F. A method for structural monitoring of multispan bridges using satellite InSAR data with uncertainty quantification and its pre-collapse application to the Albiano-Magra Bridge in Italy. *Struct. Health Monit.* **2023**, *22*, 353–371. [\[CrossRef\]](#)
- AASHTO, American Association of State Highway and Transportation Officials. *The Manual for Bridge Evaluation*; AASHTO: Washington, DC, USA, 2019.
- MIT, Ministero delle Infrastrutture e dei Trasporti. *Linee Guida per la Classificazione e Gestione del Rischio, la Valutazione della Sicurezza ed il Monitoraggio dei Ponti Esistenti*; Ministero delle Infrastrutture e dei Trasporti: Rome, Italy, 2020. (In Italian)
- Calò, M.; Ruggieri, S.; Nettis, A.; Uva, G. Multi source Interferometry Synthetic Aperture Radar for monitoring existing bridges: A case study. *Ce/papers* **2023**, *6*, 787–793. [\[CrossRef\]](#)
- Orellana, F.; Delgado Blasco, J.M.; Foulmelis, M.; D'Aranno, P.J.V.; Marsella, M.A.; Di Mascio, P. DInSAR for Road Infrastructure Monitoring: Case Study Highway Network of Rome Metropolitan (Italy). *Remote Sens.* **2020**, *12*, 3697. [\[CrossRef\]](#)
- Bordoni, M.; Bonì, R.; Colombo, A.; Lanteri, L.; Meisina, C. A methodology for ground motion area detection (GMA-D) using A-DInSAR time series in landslide investigations. *Catena* **2018**, *163*, 89–110. [\[CrossRef\]](#)
- Meisina, C.; Zucca, F.; Notti, D.; Colombo, A.; Cucchi, A.; Savio, G.; Giannico, C.; Bianchi, M. Geological interpretation of PSINSAR data at regional scale. *Sensors* **2008**, *8*, 7469–7492. [\[CrossRef\]](#)
- Calò, M.; Ruggieri, S.; Doglioni, A.; Morga, M.; Nettis, A.; Simeone, V.; Uva, G. Probabilistic-based assessment of subsidence phenomena on the existing built heritage by combining MTInSAR data and UAV photogrammetry. *Struct. Infrastruct. Eng.* **2024**, *1*–16. [\[CrossRef\]](#)
- Miano, A.; Mele, A.; Calcaterra, D.; Di Martire, D.; Infante, D.; Prota, A.; Ramondini, M. The use of satellite data to support the structural health monitoring in areas affected by slow-moving landslides: A potential application to reinforced concrete buildings. *Struct. Health Monit.* **2021**, *20*, 3265–3287. [\[CrossRef\]](#)
- Selvakumaran, S.; Plank, S.; Geiß, C.; Rossi, C.; Middleton, C. Remote monitoring to predict bridge scour failure using Interferometric Synthetic Aperture Radar (InSAR) stacking techniques. *Int. J. Appl. Earth Obs. Geoinf.* **2018**, *73*, 463–470. [\[CrossRef\]](#)
- Calò, M.; Ruggieri, S.; Nettis, A.; Uva, G. A MTInSAR-Based Early Warning System to Appraise Deformations in Simply Supported Concrete Girder Bridges. *Struct. Control Health Monit.* **2024**, *2024*, 8978782. [\[CrossRef\]](#)
- Nettis, A.; Massimi, V.; Nutricato, R.; Nitti, D.O.; Samarelli, S.; Uva, G. Satellite-based interferometry for monitoring structural deformations of bridge portfolios. *Autom. Constr.* **2023**, *147*, 104707. [\[CrossRef\]](#)
- DePrekel, K.; Bouali, E.H.; Oommen, T. Monitoring the impact of groundwater pumping on infrastructure using Geographic Information System (GIS) and Persistent Scatterer interferometry (PSI). *Infrastructures* **2018**, *3*, 57. [\[CrossRef\]](#)
- Macchiarulo, V.; Milillo, P.; Blenkinsopp, C.; Giardina, G. Monitoring deformations of infrastructure networks: A fully automated GIS integration and analysis of InSAR time-series. *Struct. Health Monit.* **2022**, *21*, 1849–1878. [\[CrossRef\]](#)
- QGIS. Spatial Without Compromise QGIS Web Site. Available online: <https://www.qgis.org/> (accessed on 14 November 2024).
- Peduto, D.; Elia, F.; Montuori, R. Probabilistic analysis of settlement-induced damage to bridges in the city of Amsterdam (The Netherlands). *Transp. Geotech.* **2018**, *14*, 169–182. [\[CrossRef\]](#)
- Del Soldato, M.; Tomás, R.; Pont, J.; Herrera, G.; Lopez-Davalillos, J.C.G.; Mora, O. A multi-sensor approach for monitoring a road bridge in the Valencia harbor (SE Spain) by SAR Interferometry (InSAR). *Rend. Online Della Soc. Geol. Ital.* **2016**, *41*, 235–238. [\[CrossRef\]](#)
- Hoppe, E.J.; Novali, F.; Rucci, A.; Fumagalli, A.; Del Conte, S.; Falorni, G.; Toro, N. Deformation monitoring of posttensioned bridges using High-Resolution satellite Remote sensing. *J. Bridge Eng.* **2019**, *24*, 04019115. [\[CrossRef\]](#)
- Giordano, P.; Turksezer, Z.; Previtali, M.; Limongelli, M. Damage detection on a historic iron bridge using satellite DInSAR data. *Struct. Health Monit.* **2022**, *21*, 2291–2311. [\[CrossRef\]](#)
- Markogiannaki, O.; Xu, H.; Chen, F.; Mitoulis, S.A.; Parcharidis, I. Monitoring of a landmark bridge using SAR interferometry coupled with engineering data and forensics. *Int. J. Remote Sens.* **2021**, *43*, 95–119. [\[CrossRef\]](#)
- Infante, D.; Di Martire, D.; Confuorto, P.; Tessitore, S.; Ramondini, M.; Calcaterra, D. Differential Sar Interferometry Technique for Control of Linear Infrastructures Affected by Ground Instability Phenomena. *Int. Arch. Photogramm. Remote Sens. Spatial Inf. Sci.* **2018**, *42*, 251–258. [\[CrossRef\]](#)
- Vaccari, A.; Batabyal, T.; Tabassum, N.; Hoppe, E.J.; Bruckno, B.S.; Acton, S.T. Integrating remote sensing data in decision support systems for transportation asset management. *Transp. Res. Rec.* **2018**, *2672*, 23–35. [\[CrossRef\]](#)
- Ciampoli, L.B.; Gagliardi, V.; Calvi, A.; D'Amico, F.; Tosti, F. Automatic network level bridge monitoring by integration of InSAR and GIS catalogues. In Proceedings of the SPIE Optical Metrology, Munich, Germany, 24–27 June 2019. [\[CrossRef\]](#)
- Cleveland, R.B.; Cleveland, W.S.; McRae, J.E.; Terpenning, I. STL: A Seasonal-Trend Decomposition Procedure based on Loess. *J. Off. Stat.* **1990**, *6*, 3–73.
- Nettis, A.; Nettis, A.; Sergio, R.; Uva, G. Corrosion-induced fragility of existing prestressed concrete girder bridges under traffic loads. *Eng. Struct.* **2024**, *314*, 118302. [\[CrossRef\]](#)
- Python. Welcome to Python.org. Available online: <https://www.python.org/> (accessed on 14 November 2024).

28. PyQGIS. Welcome to the QGIS Python API Documentation Project. Available online: <https://qgis.org/pyqgis/3.34/> (accessed on 14 November 2024).
29. Qt Designer. Qt5 Designer Manual. Available online: <https://doc.qt.io/qt-5/qtdesigner-manual.html> (accessed on 14 November 2024).
30. PyQt5. PyQt5 PyPi. Available online: <https://pypi.org/project/PyQt5/> (accessed on 14 November 2024).
31. OpenWeatherMap. Current Weather and Forecast—OpenWeatherMap. Available online: <https://openweathermap.org/> (accessed on 14 November 2024).
32. Available online: https://jmahaffy.sdsu.edu/courses/f11/math122/beamer_lectures/trig-04.pdf (accessed on 14 November 2024).
33. ReLUIS. *Linee Guida per L'utilizzo dei Dati Interferometrici Satellitari ai Fini Dell'interpretazione del Comportamento Strutturale delle Costruzioni (Draft)*; ReLUIS: Naples, Italy, 2023. (In Italian)
34. Ruggieri, S.; Nettis, A.; Raffaele, D.; Guido, B.; Uva, G. Seismic fragility and risk assessment of Reinforced Concrete bridges undergoing elastomeric bearing deformations induced by landslide. *Int. J. Bridge Eng. Manag. Res.* **2024**, *1*, 21424003-1. [CrossRef]
35. Bovenga, F.; Nutricato, R.; Refice, A.; Guerriero, L.; Chiaradia, M.T. SPINUA: A Flexible Processing Chain for ERS/ENVISAT Long Term Interferometry. European Space Agency (Special Publication): Paris, France, 2005; pp. 473–478.
36. MIT, Ministero delle Infrastrutture e dei Trasporti. *Aggiornamento delle "Norme Tecniche per le Costruzioni"*; Ministero delle Infrastrutture e dei Trasporti: Rome, Italy, 2018. (In Italian)

Disclaimer/Publisher's Note: The statements, opinions and data contained in all publications are solely those of the individual author(s) and contributor(s) and not of MDPI and/or the editor(s). MDPI and/or the editor(s) disclaim responsibility for any injury to people or property resulting from any ideas, methods, instructions or products referred to in the content.